Catalysis Science & Technology

ROYAL SOCIETY OF CHEMISTRY

PAPER

View Article Online
View Journal | View Issue





Cite this: *Catal. Sci. Technol.*, 2020, **10**, 7344

# Insights into the multiple effects of oxygen vacancies on $CuWO_4$ for photoelectrochemical water oxidation†

Wenlong Guo,[a] Ya Wang,[a] Xin Lian, *[b] Yao Nie,[a] Shijia Tian,[a] Shanshan Wang,[a] Yun Zhou*[a] and Graeme Henkelman [c]

Received 16th July 2020,
Accepted 30th August 2020

DOI: 10.1039/d0cy01430c

rsc.li/catalysis

The multiple effects of oxygen vacancies on a $CuWO_4$ photoanode for photoelectrochemical water oxidation are investigated. A shorter electron transfer time across the photoanode is obtained for $CuWO_4$ with oxygen vacancies as compared to the pristine $CuWO_4$. This provides direct evidence of the enhanced electrical conductivity for $CuWO_4$ by oxygen vacancies. The water oxidation kinetics of $CuWO_4$ is also found to be boosted by oxygen vacancies. This experimental result is further investigated using density functional theory calculations, which reveal that the activation barriers for $H_2O$ dehydrogenation on the surface of $CuWO_4$ with oxygen vacancies are much lower than those of $CuWO_4$. Interestingly, despite these advantages, oxygen vacancies are also found to be charge recombination centers on the photoanode's surface.

## 1. Introduction

Copper tungstate ($CuWO_4$) is a promising photoanode for solar water splitting due to its relatively small band gap (~2.3 eV), good photostability, and high selectivity for water oxidation.[1–4] Unfortunately, the photoelectrochemical (PEC) performance of this semiconductor is limited by its poor charge separation and transfer properties and sluggish kinetics for the oxygen evolution reaction.[5–9] Therefore, various strategies have been applied to alleviate these shortcomings, including doping with metals (Ag,[10] Fe,[11] Mo,[12] Zn,[13] Co,[14] *etc.*), depositing with cocatalysts (FeOOH,[15] CoPi,[16] NiPi,[17] MnNCN,[18] *etc.*), and constructing heterojunctions with other semiconductors (BiOI,[19] $Co_3O_4$,[20] CdS,[15] $WO_3$,[21] $BiVO_4$,[22] CuO,[23] $Mn_3O_4$,[24] *etc.*).

In addition to these efforts, the introduction of oxygen vacancies has been regarded as an effective method to enhance the PEC performance of metal oxide photoanodes.[25–28] Several groups have created oxygen vacancies on $CuWO_4$ by post-annealing the films in hydrogen or oxygen-deficient inert atmospheres.[29–32] With oxygen vacancies, higher photocurrent densities are achieved compared with the pristine films. The improvement of the PEC activity is generally attributed to an enhanced conductivity which has been explained by an increased carrier concentration as measured by Mott–Schottky curves.[29–32] Nevertheless, more studies are needed to understand the intrinsic mechanism(s) for the increased electrical conductivity by oxygen vacancies. Additionally, it is well known that the catalytic activity is closely related to the adsorption energy of the reaction molecules on the material's surface.[33,34] Oxygen vacancies will provide an unsaturated coordination environment and provide dangling bonds.[35,36] These conditions are able to facilitate the adsorption of the reactants and the charge transfer between the reactants and the catalyst.[37,38] Therefore, oxygen vacancies are expected to affect the kinetics of water oxidation on $CuWO_4$, which has rarely been studied to date. In addition, recent studies on $WO_3$ and $\alpha$-$Fe_2O_3$ photoanodes have found that oxygen vacancies can create trap states on the surface leading to serious charge recombination,[39,40] which has not been verified on $CuWO_4$.

Hence, in this work, the multiple roles of oxygen vacancies in $CuWO_4$ for PEC water oxidation are investigated using experimental measurements combined with density functional theory (DFT) calculations. It is found that oxygen vacancies are able to not only shorten the electron transfer

[a] *Chongqing Key Laboratory of Green Synthesis and Applications, College of Chemistry, Chongqing Normal University, Chongqing 401331, P. R. China. E-mail: yunzhou@cqnu.edu.cn*
[b] *College of Chemistry and Chemical Engineering, Chongqing University of Science and Technology, Chongqing, 401331, PR China. E-mail: daisylian0121@163.com*
[c] *Department of Chemistry and the Oden Institute for Computational Engineering and Sciences, The University of Texas, Austin, Texas 78712, USA*

† Electronic supplementary information (ESI) available: Film synthesis and characterization, electrochemical and photoelectrochemical measurements, DFT computational details, Raman spectra, XPS spectra, discussion of Raman and XPS spectra, photoluminescence spectra, XRD patterns, SEM morphologies, absorption spectra, PEC performances, LSV curves under dark conditions, optimized structures of (010) surfaces, discussion of structures, values of the equivalent circuit elements, and reaction rate constants. See DOI: 10.1039/d0cy01430c

time but also promote the water oxidation kinetics at the $CuWO_4$ photoanode. Furthermore, oxygen vacancies also aggravate the problem of charge recombination on the surface of $CuWO_4$. Our work deepens the understanding of the influence of oxygen vacancies on $CuWO_4$, which is helpful for designing more efficient photoanodes for solar water splitting.

## 2. Results and discussion

First, a lowering of the electron binding energies and both a weakening and broadening of the vibration spectra demonstrate the generation of oxygen vacancies in $CuWO_4$ after post-annealing in a nitrogen atmosphere (see the analyses in Fig. S1 and S2†).[29,30,32] X-ray diffraction and scanning electron microscopy show that the crystalline structure and morphology of the $CuWO_4$ films are basically unchanged after the introduction of oxygen vacancies (Fig. S3 and S4†). UV-vis spectroscopy indicates that the $N_2$-treated $CuWO_4$ has a slightly increased light harvesting ability compared with the non-treated $CuWO_4$ (Fig. S5†). There is a weak absorption beyond 700 nm for these two films. A similar phenomenon has been widely observed in $Cu^{2+}$-containing oxides and ascribed to the local ligand field excitations of $Cu^{2+}$ cations.[14,18,50–52] A band gap of 2.32 eV is assigned to both the $N_2$-treated $CuWO_4$ and the pristine $CuWO_4$ according to the Tauc plots. The calculated photocurrent density based on the absorbed photon flux of the $CuWO_4$ films before and after the $N_2$ treatment is 3.57 and 4.06 mA $cm^{-2}$, respectively.

The PEC performance of $CuWO_4$ films post-annealed in a $N_2$ atmosphere at various temperatures is evaluated and 300 °C is found to be the optimum treatment temperature (Fig. S6†). $CuWO_4$ (OV) hereinafter represents the $CuWO_4$ photoanode with $N_2$ treatment at 300 °C. A comparison of the PEC activities of $CuWO_4$ and $CuWO_4$ (OV) tested in

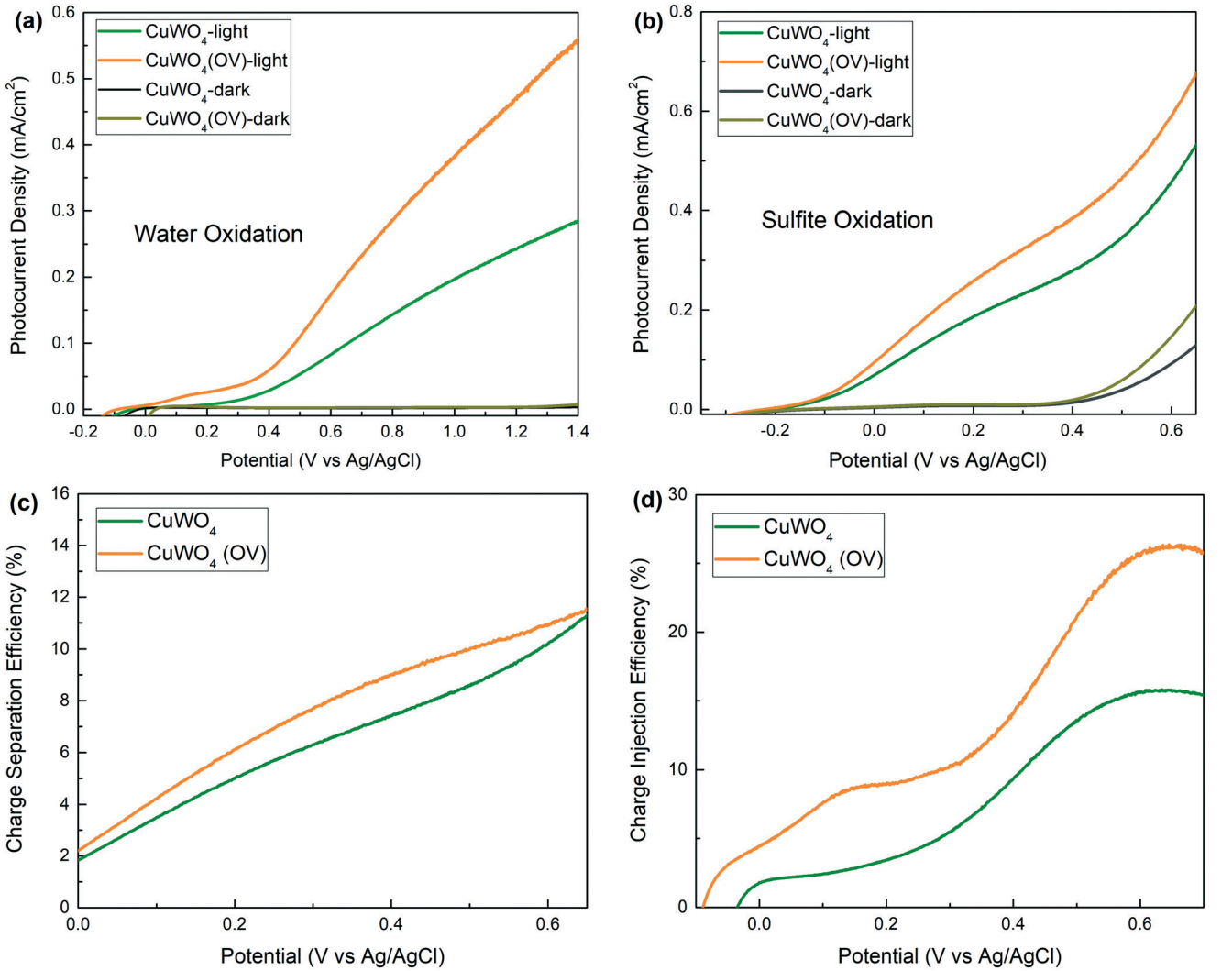


**Fig. 1** Linear sweep voltammetry (LSV) curves of $CuWO_4$ and $CuWO_4$ (OV) tested in 0.2 M $Na_2SO_4$ electrolyte (a) without and (b) with 1 M $Na_2SO_3$ as a hole scavenger (pH 7). The illumination is AM 1.5G simulated solar light with an intensity of 100 mW $cm^{-2}$. The scan rate is 25 mV $s^{-1}$. Calculated (c) charge separation and (d) charge injection efficiencies of $CuWO_4$ and $CuWO_4$ (OV).

sodium sulfate solution with and without sulfite as a hole scavenger is shown in Fig. 1a and b. For the water oxidation, $CuWO_4$ (OV) shows a higher photocurrent density and a more negative onset potential than $CuWO_4$. For the sulfite oxidation, $CuWO_4$ (OV) also exhibits a superior activity compared with $CuWO_4$. These results confirm that a moderate concentration of oxygen vacancies is able to improve the PEC performance of the $CuWO_4$ photoanodes, consistent with previous work.[29–32] In order to understand the improvement of the PEC performance, the separation efficiency of photogenerated carriers and the hole injection efficiency into the electrolyte are calculated and shown in Fig. 1c and d. Compared with $CuWO_4$, higher separation efficiencies are obtained for $CuWO_4$ (OV). This is in agreement with the higher activity for the sulfite oxidation of $CuWO_4$ (OV), that is, more holes reach the surface of $CuWO_4$ (OV) during the PEC process due to the improved charge separation. In addition, the charge injection efficiency of $CuWO_4$ (OV) is higher than that of $CuWO_4$, corresponding to an earlier onset potential of $CuWO_4$ (OV). This suggests that oxygen vacancies accelerate the charge transfer at the interface between the material surface and the electrolyte, that is, the kinetics for water oxidation is boosted. Additionally, the water oxidation stabilities of $CuWO_4$ and $CuWO_4$ (OV) are tested for 6 h at different biases and these two films show comparative and reasonable PEC stabilities (Fig. S9†).

The widely accepted explanation for the improved PEC activity of metal oxides with oxygen vacancies is that the electrical conductivity is increased due to the enhanced carrier concentration.[26,27,29,32] The Mott–Schottky measurements in this work verify this phenomenon, in which the slope of $CuWO_4$ (OV) is smaller than that of $CuWO_4$, suggesting a higher carrier concentration in $CuWO_4$ (OV). Specifically, the carrier concentrations of $CuWO_4$ and $CuWO_4$ (OV) are calculated to be $2.56 \times 10^{21}$ and $3.93 \times 10^{22}$ $cm^{-3}$, respectively. To further investigate this enhanced electrical conductivity, a controlled intensity modulated photocurrent spectroscopy (CIMPS) study was conducted to measure the charge separation and transfer properties in the bulk

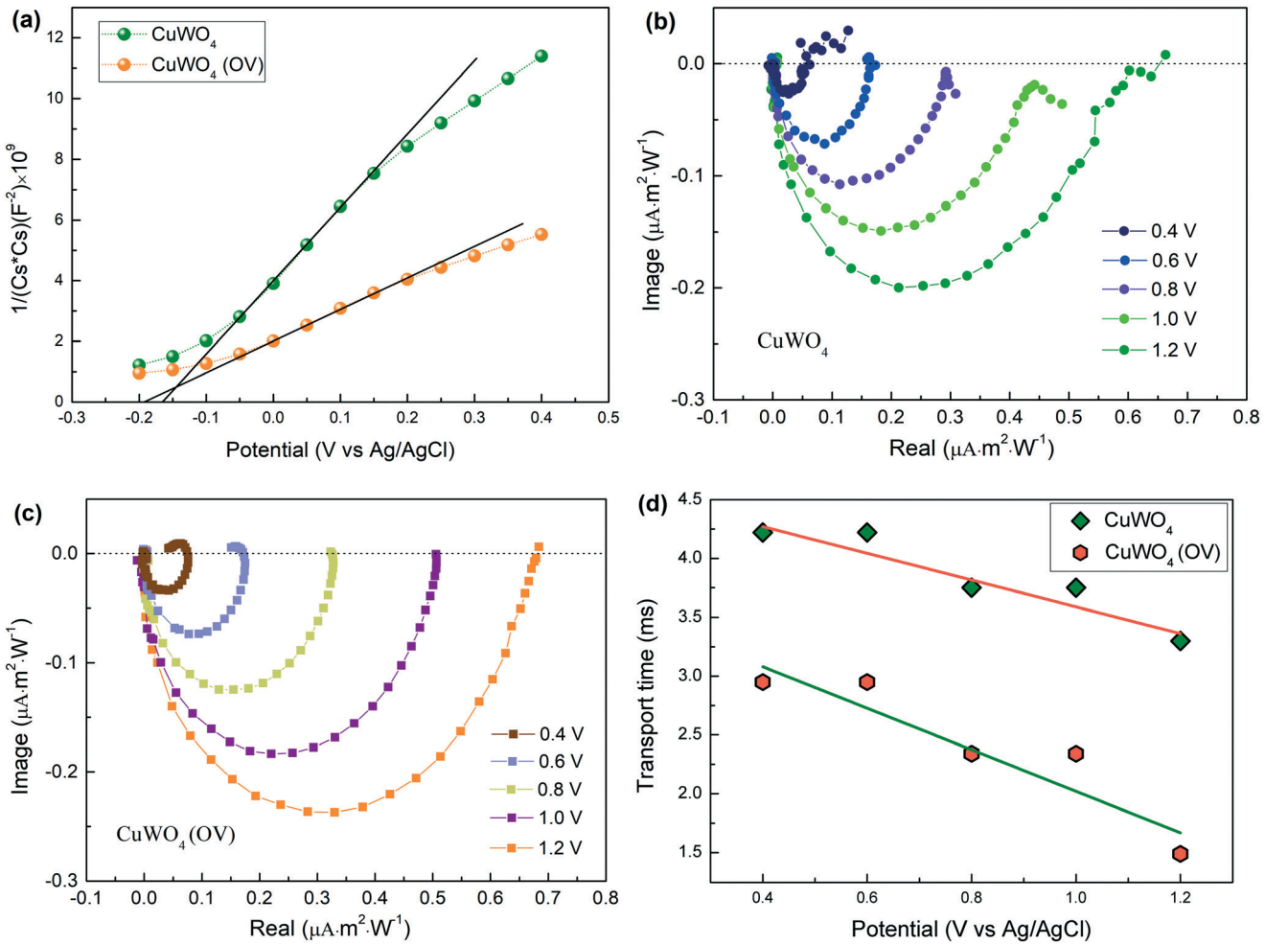


Fig. 2 (a) Mott–Schottky plots of $CuWO_4$ and $CuWO_4$ (OV) obtained in a 0.2 M $Na_2SO_4$ solution at a frequency of 3 kHz. Plots of the CIMPS complex plane of (b) $CuWO_4$ and (c) $CuWO_4$ (OV) measured in a 0.2 M $Na_2SO_4$ solution at various biases under a light intensity of 300 mW $cm^{-2}$ ($\lambda$ = 365 nm). (d) Calculated electron transport time of $CuWO_4$ and $CuWO_4$ (OV) at various applied potentials.

 

material. The CIMPS Nyquist plots of $CuWO_4$ and $CuWO_4$ (OV) at various applied potentials illuminated by a 365 nm LED are shown in Fig. 2b and c. For both photoanodes, the radii of the semicircular shapes in the third and fourth quadrants gradually increase with the enhancement of the biases, indicating that more holes are collected.[41,42] Additionally, the transfer time of photogenerated carriers is useful for evaluating the charge transport properties of the inorganic photoanodes.[43,44] The electron transfer times of $CuWO_4$ and $CuWO_4$ (OV) at various applied potentials are calculated based on the frequency of the lowest point in the CIMPS complex plane as shown in Fig. 2d. These values give an estimation of the average transfer time of photogenerated electrons from the surface to the substrate across the photoanodes with similar film thickness.[42] Apparently, the electron transfer times of $CuWO_4$ (OV) are generally shorter than those of $CuWO_4$, demonstrating the better carrier mobility of the $CuWO_4$ (OV) photoanode.

The charge transfer properties across the electrode/electrolyte interface, which are closely related to the water oxidation kinetics of the material, are explored using electrochemical impedance spectroscopy (Fig. 3a). The equivalent circuit as shown in the inset of Fig. 3a is applied to interpret the Nyquist plots, where $R_s$ is the solution resistance, CPE is the constant phase element, and $R_{ct}$ is the charge transfer resistance between the surface and the electrolyte. It is found that the arc in the Nyquist diagram for $CuWO_4$ (OV) is smaller than that for $CuWO_4$, showing that the charge transfer resistance is smaller for $CuWO_4$ (OV).[45] Specifically, the $R_{ct}$ values for $CuWO_4$ (OV) and $CuWO_4$ are 1190 and 1795 Ω, respectively (Table S1†). These results are consistent with the calculated injection efficiencies for $CuWO_4$ and $CuWO_4$ (OV) shown in Fig. 1d. A lower overpotential for electrochemical water oxidation on $CuWO_4$ (OV) compared to that on $CuWO_4$ under dark conditions also demonstrates the faster kinetics for water oxidation of the electrode with oxygen vacancies (Fig. S7†).

In order to further understand the improved kinetics, the dissociation pathways and activation barriers of the water molecule on the (010) surface of $CuWO_4$ and $CuWO_4$ with

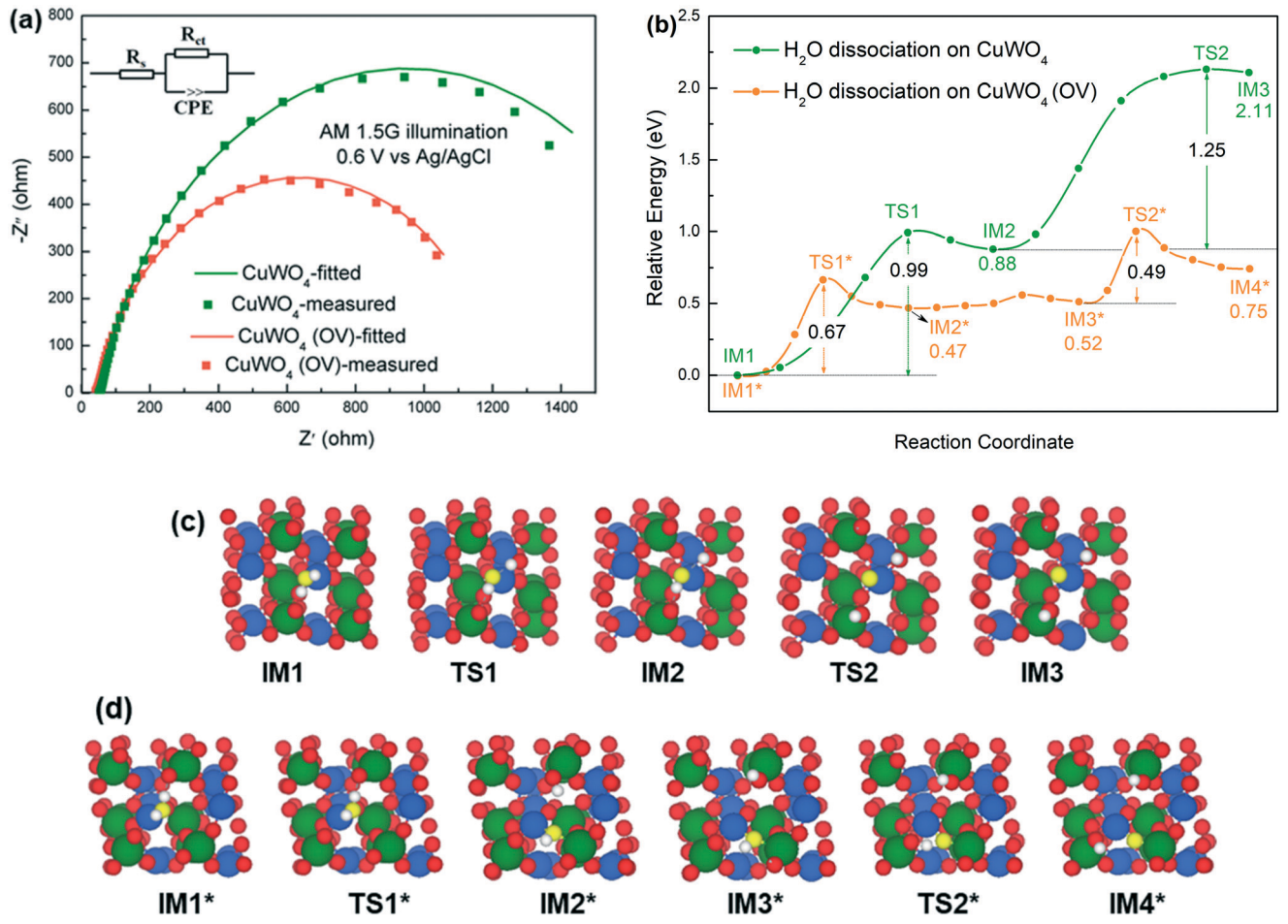


**Fig. 3** (a) EIS plots of $CuWO_4$ and $CuWO_4$ (OV) in a 0.2 M $Na_2SO_4$ solution under AM 1.5 G illumination (100 mW $cm^{-2}$) at 0.6 V *vs.* Ag/AgCl. The solid lines are fitted using the Zview software; the inset is the equivalent circuit. (b) MEP plots for the $H_2O$ dehydrogenation pathway on $CuWO_4$ and $CuWO_4$ (OV). The structures of intermediates and transition states involved in the reaction pathways of (c) $CuWO_4$ and (d) $CuWO_4$ (OV). Cu, W, and O are blue, green, and red spheres, respectively. The adsorbed O and H atoms are yellow and white, respectively.

oxygen vacancies are calculated using DFT. A detailed discussion of the model structures is provided in Fig. S8.† The (010) facet of the triclinic $CuWO_4$ considered here is one of the dominant characteristic facets and has been demonstrated to be a PEC active surface.[46,47] The minimum energy paths (MEPs) for $H_2O$ dehydrogenation on the (010) facet of $CuWO_4$ and $CuWO_4$ (OV) are shown in Fig. 3b. For $CuWO_4$, the dissociation energy barrier from $H_2O$ to OH is calculated to be 0.99 eV, while the activation energy from OH to O is 1.25 eV. These calculations suggest that the dehydrogenation of OH is more kinetically difficult than the dehydrogenation of $H_2O$ on the $CuWO_4$ surface. For $CuWO_4$ (OV), the scission barrier of one of the O–H bonds in $H_2O$ is 0.67 eV, while the scission barrier of the resulting OH group is 0.49 eV, indicating that the second proton more easily dissociates than the first one for the water molecule on $CuWO_4$ (OV). In comparison, the dehydrogenation reactions of $H_2O$ and OH are kinetically more favorable on the $CuWO_4$ surface with oxygen vacancies than on the stoichiometric $CuWO_4$ surface. The reaction rate constants of the elementary reactions are calculated using the activation barriers (Table S2†). At 298.15 K, the rate constants for the $H_2O$ and OH dehydrogenation reactions on $CuWO_4$ are $2.10 \times 10^{-4}$ and $8.77 \times 10^{-9}$ $s^{-1}$, respectively. On $CuWO_4$ (OV), the rate constants for these two elementary steps are $5.17 \times 10^{1}$ and $5.57 \times 10^{4}$ $s^{-1}$, respectively. Apparently, the rate for the $H_2O$ dissociation on $CuWO_4$ (OV) is much faster than that on $CuWO_4$, indicating superior water oxidation kinetics for $CuWO_4$ (OV). The structures of the intermediates and transition states involved in the $H_2O$ dehydrogenation pathways are shown in Fig. 3c and d. For both $CuWO_4$ and $CuWO_4$ (OV), $H_2O$ adsorbs on the top site of the Cu atom through the O atom. The first proton migrates to an adjacent O atom in the lattice concerted with one O–H bond breakage. Subsequently, the second H bond dissociates and the H atom moves to another lattice oxygen atom, resulting in a metal-

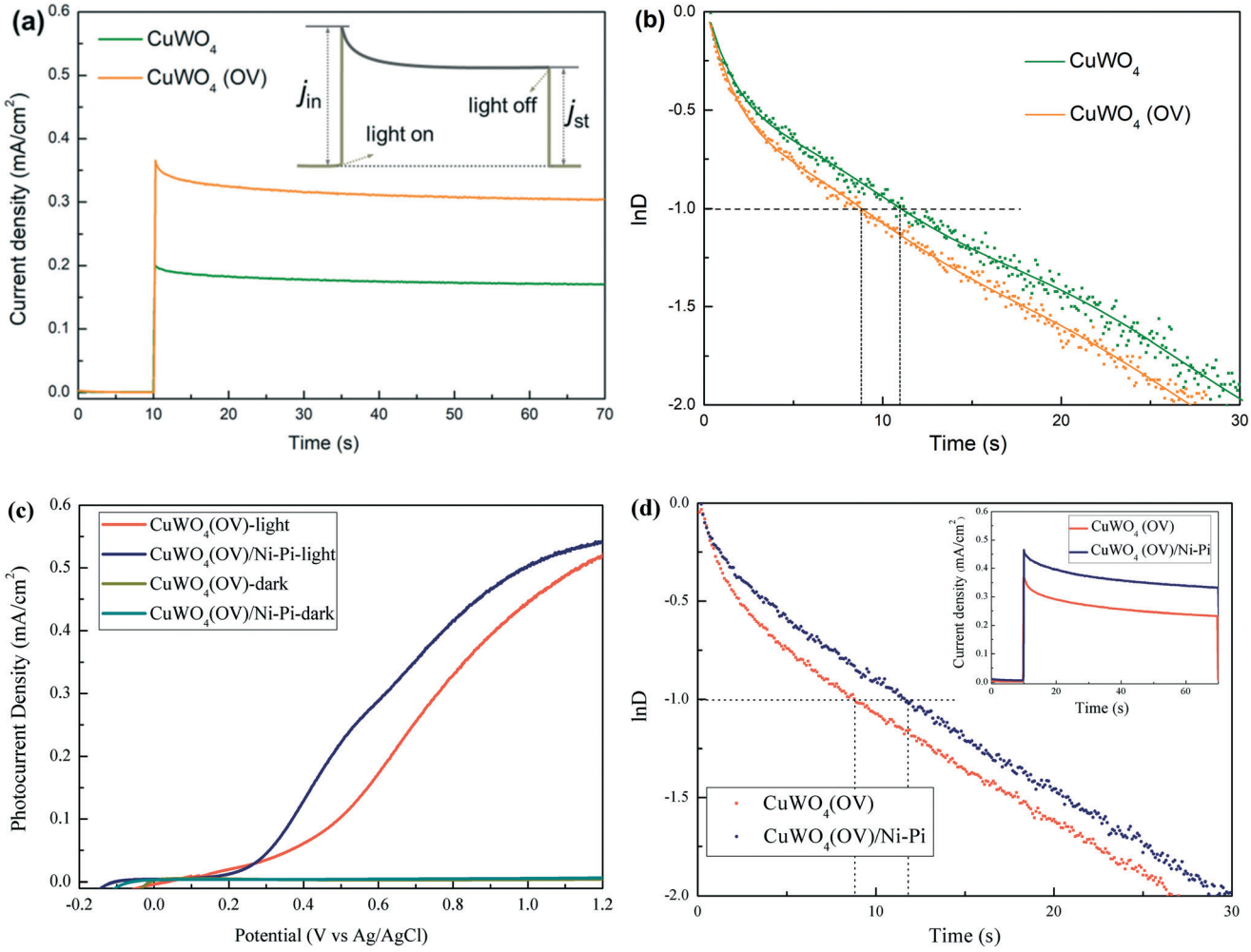


**Fig. 4** (a) Transient photocurrent responses of the $CuWO_4$ and $CuWO_4$ (OV) films measured at 0.9 V *vs.* Ag/AgCl in 0.2 M $Na_2SO_4$ electrolyte under AM 1.5G illumination (100 mW $cm^{-2}$). (b) Normalized plots of the current–time dependence of the anodic transients for the $CuWO_4$ and $CuWO_4$ (OV) films. (c) LSV curves of $CuWO_4$ (OV) and $CuWO_4$ (OV)/Ni-Pi tested in 0.2 M $Na_2SO_4$ electrolyte under AM 1.5G illumination (100 mW $cm^{-2}$). (d) Normalized plots of the current–time dependence of the anodic transients for the $CuWO_4$ (OV) and $CuWO_4$ (OV)/Ni-Pi films. The inset is the transient photocurrent responses of the $CuWO_4$ (OV) and $CuWO_4$ (OV)/Ni-Pi films measured at 0.9 V *vs.* Ag/AgCl in 0.2 M $Na_2SO_4$ electrolyte.

 

oxo species. It is worth noting that the $H_2O$ adsorption energies on $CuWO_4$ and $CuWO_4$ (OV) are −1.19 and −1.54 eV, respectively. The relatively strong interaction between $H_2O$ and $CuWO_4$ (OV) facilitates the dehydrogenation reactions.

Despite these advantages, the effect of oxygen vacancies on surface charge recombination, which is a competitive route with the water oxidation reaction for photogenerated carriers, is examined using chronoamperometry.[48,49] The transient photocurrent responses of the $CuWO_4$ and $CuWO_4$ (OV) films are shown in Fig. 4a. In the inset of Fig. 4a, $j_{in}$ is the initial photocurrent and $j_{st}$ is the steady-state photocurrent. A normalized parameter ($D$) is defined as follows:

$$D = (j_t - j_{st})/(j_{in} - j_{st})$$

where $j_t$ is the time-dependent photocurrent. A normalized plot is made with $\ln(D)$ as the $y$-axis and reaction time as the $x$-axis. The transient time constant ($\tau$) is defined as the time at which $\ln(D)$ is equal to −1. By calculation, the $\tau$ value for the $CuWO_4$ and $CuWO_4$ (OV) films is 10.9 and 8.8 s, respectively, suggesting that $CuWO_4$ (OV) suffers more from surface charge recombination than $CuWO_4$. To further verify this inference, nickel phosphate (Ni-Pi) which can restrain the surface states is deposited on $CuWO_4$ and $CuWO_4$ (OV),[17,53] which is characterized using the XPS measurement (Fig. S10†). On the one hand, Ni-Pi as an oxygen evolution catalyst enhances the PEC activity for both $CuWO_4$ (OV) and $CuWO_4$ (Fig. 4c and S11a†), consistent with previous work.[17,53] On the other hand, Ni-Pi obviously prolongs the transient time constant for $CuWO_4$ (OV) as shown in Fig. 4d, while the $\tau$ values for $CuWO_4$ before and after the decoration of Ni-Pi are similar (Fig. S11b†). This further suggests that oxygen vacancies can create trap states on the surface of $CuWO_4$, which aggravates the charge recombination.

## 3. Conclusion

In this work, oxygen vacancies are introduced into a $CuWO_4$ film by $N_2$ treatment and their multiple roles in this photoanode for PEC water oxidation are investigated. With oxygen vacancies, both the charge separation and injection efficiencies of $CuWO_4$ are boosted. Aside from the increase of the carrier concentration, the electron transfer time across the photoanode for $CuWO_4$ (OV) is measured to be shorter than that for $CuWO_4$. This is direct evidence of the improved electrical conductivity caused by oxygen vacancies. In addition, the water oxidation kinetics of $CuWO_4$ is improved by oxygen vacancies, which is studied using DFT calculations. The activation energies for the $H_2O$ dehydrogenation on $CuWO_4$ (OV) are much lower than those on $CuWO_4$. Despite these advantages, it is found that oxygen vacancies also aggravate the charge recombination on the surface of $CuWO_4$. Our work highlights the multiple roles of oxygen vacancies in the $CuWO_4$ photoanode for PEC water oxidation, which is useful for the design and synthesis of more efficient photocatalysts containing oxygen vacancies for solar water splitting.

## Conflicts of interest

There are no conflicts to declare.

## Acknowledgements

We gratefully acknowledge the Texas Advanced Computing Center for computational resources, and funding from the National Natural Science Foundation of China (Grant No. 21903009) and the Science and Technology Research Program of Chongqing Municipal Education Commission (Grant No. KJQN201800515 and KJQN201801525). PhD Initial Funding of Chongqing Normal University (Grant No. 17XLB015).

## References

1 J. E. Yourey and B. M. Bartlett, Electrochemical Deposition and Photoelectrochemistry of $CuWO_4$, A Promising Photoanode for Water Oxidation, *J. Mater. Chem.*, 2011, **21**, 7651–7660.
2 Y. C. Chang, A. Braun, A. Deangelis, J. Kaneshiro and N. Gaillard, Effect of Thermal Treatment on the Crystallographic, Surface Energetics, and Photoelectrochemical Properties of Reactively Cosputtered Copper Tungstate for Water Splitting, *J. Phys. Chem. C*, 2011, **115**, 25490–25495.
3 U. M. García-Pérez, A. Martínez-de la Cruz and J. Peral, Transition Metal Tungstates Synthesized by Co-Precipitation Method: Basic Photocatalytic Properties, *Electrochim. Acta*, 2012, **81**, 227–232.
4 J. E. Yourey, K. J. Pyper, J. B. Kurtz and B. M. Bartlett, Chemical Stability of $CuWO_4$ for Photoelectrochemical Water Oxidation, *J. Phys. Chem. C*, 2013, **117**, 8708–8718.
5 K. J. Pyper, J. E. Yourey and B. M. Bartlett, Reactivity of $CuWO_4$ in Photoelectrochemical Water Oxidation Is Dictated by a Midgap Electronic State, *J. Phys. Chem. C*, 2013, **117**, 24726–24732.
6 J. C. Hilla and K. S. Choi, Synthesis and Characterization of High Surface Area $CuWO_4$ and $Bi_2WO_6$ Electrodes for Use as Photoanodes for Solar Water Oxidation, *J. Mater. Chem. A*, 2013, **1**, 5006–5014.
7 Y. Gao and T. W. Hamann, Elucidation of $CuWO_4$ Surface States During Photoelectrochemical Water Oxidation, *J. Phys. Chem. Lett.*, 2017, **8**, 2700–2704.
8 Y. Gao and T. W. Hamann, Quantitative Hole Collection for Photoelectrochemical Water Oxidation with $CuWO_4$, *Chem. Commun.*, 2017, **53**, 1285–1288.
9 C. M. Tian, M. Jiang, D. Tang, L. Qiao, H. Y. Xiao, F. E. Oropeza, J. P. Hofmann, E. J. M. Hensen, A. Tadich, W. Li, D. C. Qi and K. H. L. Zhang, Elucidating the Electronic Structure of $CuWO_4$ Thin Films for Enhanced Photoelectrochemical Water Splitting, *J. Mater. Chem. A*, 2019, **7**, 11895–11907.
10 H. Zhang, P. Yilmaz, J. O. Ansari, F. F. Khan, R. Binions, S. Krause and S. Dunn, Incorporation of Ag nanowires in

$CuWO_4$ for Improved Visible Light-Induced Photoanode Performance, *J. Mater. Chem. A*, 2015, **3**, 9638–9644.

11 D. Bohraa and W. A. Smith, Improved Charge Separation via Fe-doping of Copper Tungstate Photoanodes, *Phys. Chem. Chem. Phys.*, 2015, **17**, 57–66.

12 J. J. Yang, C. Li and P. Diao, Molybdenum Doped $CuWO_4$ Nanoflake Array Films as An Efficient Photoanode for Solar Water Splitting, *Electrochim. Acta*, 2019, **308**, 195–205.

13 J. E. Yourey, J. B. Kurtz and B. M. Bartlett, Structure, Optical Properties, and Magnetism of the Full $Zn_{1-x}Cu_xWO_4$ ($0 \leq X \leq 1$) Composition Range, *Inorg. Chem.*, 2012, **51**, 10394–10401.

14 C. R. Lhermitte and B. M. Bartlett, Advancing the Chemistry of $CuWO_4$ for Photoelectrochemical Water Oxidation, *Acc. Chem. Res.*, 2016, **49**, 1121–1129.

15 M. Zhou, Z. H. Liu, X. F. Li and Z. F. Liu, Promising Three-Dimensional Flower like $CuWO_4$ Photoanode Modified with CdS and FeOOH for Efficient Photoelectrochemical Water Splitting, *Ind. Eng. Chem. Res.*, 2018, **57**, 6210–6217.

16 S. Chen, M. N. Hossain and A. C. Chen, Significant Enhancement of the Photoelectrochemical Activity of $CuWO_4$ by using a Cobalt Phosphate Nanoscale Thin Film, *ChemElectroChem*, 2018, **5**, 523–530.

17 X. Q. Xiong, L. Y. Fan, G. H. Chen, Y. Wang, C. L. Wu, D. Chen, Y. Lin, T. D. Li, S. Fu and S. B. Ren, Boosting Water Oxidation Performance of $CuWO_4$ Photoanode by Surface Modification of Nickel Phosphate, *Electrochim. Acta*, 2019, **328**, 135125.

18 M. Davi, M. Mann, Z. L. Ma, F. L. Schrader, A. Drichel, S. Budnyk, A. Rokicinska, P. Kustrowski, R. Dronskowski and A. Slabon, An MnNCN-Derived Electrocatalyst for $CuWO_4$ Photoanodes, *Langmuir*, 2018, **34**, 3845–3852.

19 M. Zhou, Z. G. Guo, Q. G. Song, X. F. Li and Z. F. Liu, Improved Photoelectrochemical Response of $CuWO_4$/BiOI p-n Heterojunction Embedded with Plasmonic Ag Nanoparticles, *Chem. Eng. J.*, 2019, **370**, 218–227.

20 Z. F. Liu, Q. G. Song, M. Zhou, Z. G. Guo, J. H. Kang and H. Y. Yan, Synergistic Enhancement of Charge Management and Surface Reaction Kinetics by Spatially Separated Cocatalysts and p-n Heterojunctions in Pt/$CuWO_4$/$Co_3O_4$ Photoanode, *Chem. Eng. J.*, 2019, **374**, 554–563.

21 J. E. Yourey, J. B. Kurtz and B. M. Bartlett, Water Oxidation on a $CuWO_4$–$WO_3$ Composite Electrode in the Presence of $[Fe(CN)_6]^{3-}$: Toward Solar Z-Scheme Water Splitting at Zero Bias, *J. Phys. Chem. C*, 2012, **116**, 3200–3205.

22 S. K. Pilli, T. G. Deutsch, T. E. Furtak, L. D. Brown, J. A. Turner and A. M. Herring, $BiVO_4$/$CuWO_4$ Heterojunction Photoanodes for Efficient Solar Driven Water Oxidation, *Phys. Chem. Chem. Phys.*, 2013, **15**, 3273–3278.

23 J. Y. Zheng, G. Song, C. W. Kim and Y. S. Kang, Facile Preparation of p-CuO and p-CuO/n-$CuWO_4$ Junction Thin Films and Their Photoelectrochemical Properties, *Electrochim. Acta*, 2012, **69**, 340–344.

24 K. Z. Li, C. Y. Zhang, X. Li, Y. K. Du, P. Yang and M. S. Zhu, A Nanostructured $CuWO_4$/$Mn_3O_4$ with p/n Heterojunction as Photoanode toward Enhanced Water Oxidation, *Catal. Today*, 2019, **335**, 173–179.

25 S. Hoang, S. P. Berglund, N. T. Hahn, A. J. Bard and C. B. Mullins, Enhancing Visible Light Photo-oxidation of Water with $TiO_2$ Nanowire Arrays via Cotreatment with $H_2$ and $NH_3$: Synergistic Effects between $Ti^{3+}$ and N, *J. Am. Chem. Soc.*, 2012, **134**, 3659–3662.

26 G. M. Wang, H. Y. Wang, Y. C. Ling, Y. C. Tang, X. Y. Yang, R. C. Fitzmorris, C. C. Wang, J. Z. Zhang and Y. Li, Hydrogen-Treated $TiO_2$ Nanowire Arrays for Photoelectrochemical Water Splitting, *Nano Lett.*, 2011, **11**, 3026–3033.

27 G. M. Wang, Y. C. Ling, H. Y. Wang, X. Y. Yang, C. C. Wang, J. Z. Zhang and Y. Li, Hydrogen-Treated $WO_3$ Nanoflakes Show Enhanced Photostability, *Energy Environ. Sci.*, 2012, **5**, 6180–6187.

28 X. B. Chen, L. Liu, P. Y. Yu and S. S. Mao, Increasing Solar Absorption for Photocatalysis with Black Hydrogenated Titanium Dioxide Nanocrystals, *Science*, 2011, **331**, 746–750.

29 Y. L. Tang, N. N. Rong, F. L. Liu, M. S. Chu, H. M. Dong, Y. H. Zhang and P. Xiao, Enhancement of the Photoelectrochemical Performance of $CuWO_4$ Films for Water Splitting by Hydrogen Treatment, *Appl. Surf. Sci.*, 2016, **361**, 133–140.

30 W. L. Guo, Z. Y. Duan, N. Mabayoje, W. D. Chemelewski, P. Xiao, G. Henkelman, Y. H. Zhang and C. B. Mullinsa, Improved Charge Carrier Transport of Hydrogen-Treated Copper Tungstate: Photoelectrochemical and Computational Study, *J. Electrochem. Soc.*, 2016, **163**, H970–H975.

31 D. Y. Hu, P. Diao, D. Xu, M. Y. Xia, Y. Gu, Q. Y. Wu, C. Li and S. B. Yang, Copper(II) Tungstate Nanoflake Array Films: Sacrificial Template Synthesis, Hydrogen Treatment, and Their Application as Photoanodes in Solar Water Splitting, *Nanoscale*, 2016, **8**, 5892–5901.

32 Z. L. Ma, O. Linnenberg, A. Rokicinska, P. Kustrowski and A. Slabon, Augmenting the Photocurrent of $CuWO_4$ Photoanodes by Heat Treatment in the Nitrogen Atmosphere, *J. Phys. Chem. C*, 2018, **122**, 19281–19288.

33 J. X. Yang, D. E. Wang, X. Zhou and C. Li, A Theoretical Study on the Mechanism of Photocatalytic Oxygen Evolution on $BiVO_4$ in Aqueous Solution, *Chem. – Eur. J.*, 2013, **19**, 1320–1326.

34 Z. Y. Duan and G. Henkelman, Theoretical Resolution of the Exceptional Oxygen Reduction Activity of Au(100) in Alkaline Media, *ACS Catal.*, 2019, **9**, 5567–5573.

35 M. Guan, C. Xiao, J. Zhang, S. Fan, R. An, Q. Cheng, J. Xie, M. Zhou, B. Ye and Y. Xie, Vacancy Associates Promoting Solar-Driven Photocatalytic Activity of Ultrathin Bismuth Oxychloride Nanosheets, *J. Am. Chem. Soc.*, 2013, **135**, 10411–10417.

36 H. Li, J. Shang, H. Zhu, Z. Yang, Z. Ai and L. Zhang, Oxygen Vacancy Structure Associated Photocatalytic Water Oxidation of BiOCl, *ACS Catal.*, 2016, **6**, 8276–8285.

37 M. J. Yang, H. C. He, J. Y. Du, H. R. Peng, G. L. Ke and Y. Zhou, Insight into the Kinetic Influence of Oxygen Vacancies on the $WO_3$ Photoanodes for Solar Water Oxidation, *J. Phys. Chem. Lett.*, 2019, **10**, 6159–6165.

38 H. Li, J. Shang, Z. Ai and L. Zhang, Efficient Visible Light Nitrogen Fixation with BiOBr Nanosheets of Oxygen

 

Vacancies on the Exposed {001} Facets, *J. Am. Chem. Soc.*, 2015, **137**, 6393.

39 J. J. Zhang, X. X. Chang, C. C. Li, A. Li, S. S. Liu, T. Wang and J. L. Gong, $WO_3$ Photoanodes with Controllable Bulk and Surface Oxygen Vacancies for Photoelectrochemical Water Oxidation, *J. Mater. Chem. A*, 2018, **6**, 3350–3354.

40 Z. L. Wang, X. Mao, P. Chen, M. Xiao, S. A. Monny, S. C. Wang, M. Konarova, A. J. Du and L. Z. Wang, Understanding the Roles of Oxygen Vacancy in Hematite based Photoelectrochemical Process, *Angew. Chem.*, 2019, **131**, 1042–1046.

41 Y. Gao and T. W. Hamann, Quantitative Hole Collection for Photoelectrochemical Water Oxidation with $CuWO_4$, *Chem. Commun.*, 2017, **53**, 1285–1288.

42 T. Oekermann, D. S. Zhang, T. Yoshida and H. Minoura, Electron Transport and Back Reaction in Nanocrystalline $TiO_2$ Films Prepared by Hydrothermal Crystallization, *J. Phys. Chem. B*, 2004, **108**, 2227–2235.

43 Y. P. Zhang, Y. Li, D. Q. Ni, Z. W. Chen, X. Wang, Y. Y. Bu and J. P. Ao, Improvement of $BiVO_4$ Photoanode Performance During Water Photo-Oxidation Using Rh-Doped $SrTiO_3$ Perovskite as a Co-Catalyst, *Adv. Funct. Mater.*, 2019, **29**, 1902101.

44 I. Rodríguez-Gutierrez, E. Djatoubai, M. Rodríguez-Perez, J. Z. Su, G. Rodríguez-Gattorno, L. Vayssieres and G. Oskam, Photoelectrochemical Water Oxidation at FTO|$WO_3$@$CuWO_4$ and FTO|$WO_3$@$CuWO_4$|$BiVO_4$ Heterojunction Systems: An IMPS Analysis, *Electrochim. Acta*, 2019, **308**, 317–327.

45 H. C. He, S. P. Berglund, A. J. E. Rettie, W. D. Chemelewski, P. Xiao, Y. H. Zhang and C. B. Mullins, Synthesis of $BiVO_4$ Nanoflake Array Films for Photoelectrochemical Water Oxidation, *J. Mater. Chem. A*, 2014, **2**, 9371–9379.

46 J.-P. Doumerc, J. Hejtmanek, J.-P. Chaminade, M. Pouchard and M. Krussanov, A Photoelectrochemical Study of $CuWO_4$ Single Crystals, *Phys. Stat. Sol.*, 1984, **82**, 285–294.

47 W. C. Ding, X. N. Wu and Q. F. Lu, Structure and Photocatalytic Activity of Thin-Walled $CuWO_4$ Nanotubes: An Experimental and DFT study, *Phys. Status Solidi A*, 2019, **253**, 323–326.

48 J. T. Li, S. K. Cushing, P. Zheng, F. Meng, D. Chu and N. Q. Wu, Plasmon-Induced Photonic and Energy-Transfer Enhancement of Solar Water Splitting by a Hematite Nanorod Array, *Nat. Commun.*, 2013, **4**, 2651.

49 X. H. Zhong, H. C. He, M. J. Yang, G. L. Ke, Z. Y. Zhao, F. Q. Dong, B. W. Wang, Y. Q. Chen, X. Y. Shi and Y. Zhou, $In^{3+}$-doped $BiVO_4$ Photoanodes with Passivated Surface States for Photoelectrochemical Water Oxidation, *J. Mater. Chem. A*, 2018, **6**, 10456.

50 C. M. Jiang, M. Farmand, C. H. Wu, Y. S. Liu, J. H. Guo, W. S. Drisdell, J. K. Cooper and I. D. Sharp, Electronic Structure, Optoelectronic Properties, and Photoelectrochemical Characteristics of $\gamma$-$Cu_3V_2O_8$ Thin Films, *Chem. Mater.*, 2017, **29**, 3334–3345.

51 W. L. Guo, X. Lian, Y. Nie, M. C. Hu, L. M. Wu, H. H. Gao and T. Wang, Facile Growth of $\beta$-$Cu_2V_2O_7$ Thin Films and Characterization for Photoelectrochemical Water Oxidation, *Mater. Lett.*, 2020, **258**, 126842.

52 F. P. Koffyberg and F. A. Benko, A Photoelectrochemical Determination of the Position of the Conduction and Valence Band Edges of P-Type CuO, *J. Appl. Phys.*, 1982, **53**, 1173–1177.

53 J. Wang, J. Y. Yang, Z. Y. Zheng, T. B. Lu and W. H. Gao, The Role of Thin NiPi Film for Enhancing Solar Water Splitting performance of Ti Doped Hematite, *Appl. Catal., B*, 2017, **218**, 277–286.